Iranian Journal of Catalysis 9(4), 2019, 357-368

IRANIAN JOURNAL OF CATALYSIS

Oxidation of greenhouse gases, CH_4 and CO, over $LaMn_xNi_{1-x}O_{3\pm\delta}$ mixed oxide

Farhad Banisharif[a,*], Mohammad Reza Dehghani[a], Golshan Mazloom[b], Yahya Hojatpanah[a]

[a]*Chemical Engineering Department, School of Chemical, Petroleum and Gas Engineering, Iran University of Science and Technology, Tehran, Iran.*

[b]*Department of Chemical Engineering, Faculty of Engineering, University of Mazandaran, Babolsar, Iran.*

Received 11 March 2019; received in revised form 15 July 2019; accepted 1 September 2019

ABSTRACT

The performance of $LaMn_xNi_{1-x}O_{3\pm\delta}$ perovskite mixed oxides (x = 0, 0.1, 0.3, 0.5, 0.7, 0.9, 1) which were prepared by different methods, the Pechini and sol-gel methods in the oxidation of greenhouse gases, CH_4 and CO, has been investigated. All samples were characterized using Fourier transform infrared spectroscopy, X-ray diffraction, scanning electron microscopy and N_2 adsorption. The results showed that Pechini samples are more active and stable than the sol-gel samples. The partially substituted Ni samples exhibited higher catalytic performance as compared to the $LaMnO_3$ due to the structural defects. But, the high substitution of Ni gradually deforms the structure to rhombohedra, decreases surface area and reduces the number of active Mn sites. Therefore, the catalytic performance passes through a maximum with respect to Ni content. $LaMn_{0.3}Ni_{0.7}O_{3\pm\delta}$ prepared by the Pechini method is more active than others in the oxidation of CH_4 and CO.

***Keywords**: Perovskite mixed oxide, $LaMn_xNi_{1-x}O_{3\pm\delta}$, Greenhouse gas, Methane combustion, CO oxidation.*

1. Introduction

In recent years, natural gas, particularly in the form of CH_4, has attracted much attention as fuel for vehicles and industrial processes due to its cost effectiveness, high efficiency and environmental advantages. However, emissions of unburnt CH_4 as a powerful greenhouse gas and also CO (another greenhouse gas and the source of human poisoning) especially in the exhaust flue gas of the motor vehicles are expected to be a big concern in the future [1, 2]. A promising way for CH_4 and CO removal from flue gas of the vehicles is using catalytic converters [3-7]. Over the last decades, intensive researches have been focused on the perovskite mixed oxide catalyst which is cheaper with acceptable activity and resistance to deactivation compared to traditional noble based catalysts [3-11].

The perovskite-type catalyst has a well-defined structure with the general formula of ABO_3 in which A usually is Lanthanide (La, Gd, Pr) and B is transition metal ion (Mn, Cr, Fe, Ni and Co). The thermal stability and catalytic activity of perovskite type catalysts have been found to depend on the nature of B cation. Hence the B cation selection is very important in the design of the catalyst and modification of their performance. Mn- and Ni-based perovskite catalysts prepared by different methods have been investigated widely in greenhouse gas oxidation. Ziaei-Azad et al. [12] have investigated the catalytic performance of different $LaBO_3$ (B= Mn, Fe, Co and Ni) perovskites for the oxidation of CH_4 and CO. Ding et al. [13] have studied the catalytic performance of $LaMnO_3$ catalyst in methane combustion. The authors have focused on the improvement of their catalyst with a new etching technology. Einaga et al. [14] have studied the CO oxidation over $LaBO_3$ (B= Mn, Fe, Co) catalysts under microwave irradiation.

Interestingly, perovskite oxides display remarkable structural capability for doping and/or partially substitution of metal in A and/or B sites which can result in enhancement of catalytic activity and stability [15]. Different partially substituted perovskite catalysts such as $La_{1-x}M_xMnO_3$ (M=Ag, Sr, Ce, La) [16], $LaNi_{1-x}Co_xO_3$ [17], $La_{1-x}Ce_xMnO_3$ [18] and $La_{0.8}Sr_{0.2}Co_{0.5}M_{0.5}O_3$ (M=Co, Ni, Cu) [19] have been used for the greenhouse gases combustion. The preparation, structure, illumination and application of perovskite catalysts have been reviewed, in detail [20-24].

*Corresponding author.
E-mail address: f_banisharif@alumni.iust.ac.ir (F. Banisharif)

To the best of our knowledge, the application of $LaMn_xNi_{1-x}O_3$ in CO and CH_4 oxidation has not been reported yet. However, B partially substituted by lower valency cations can lead to defect formation in the perovskite structure as oxygen vacancies or variation oxidation state of B cation that can influence on the oxygen mobility and catalytic performance [25].

Despite the advantages of perovskites proven in different reactions, these catalysts suffer from their low surface area (usually less than 10 m^2/g). One of the factors influencing the surface area is the preparation method. Many attempts have been made for improving the surface area by different methods including Pechini, hydrothermal, impregnation, urea precipitation, sol-gel, auto combustion [20].

In this work, different $LaMn_xNi_{1-x}O_3$ perovskite catalysts with x = 0, 0.1, 0.3, 0.5, 0.7, 0.9, 1 have been synthesized with sol-gel and Pechini methods and characterized using different techniques. The catalytic performance of synthesized catalysts has been investigated and compared in CO and CH_4 combustion. The effects of the preparation method and partial substitution of Mn by Ni on the structure and catalytic activity have been discussed.

2. Experimental

2.1. Preparation of catalyst

The $LaMn_xNi_{1-x}O_3$ catalysts with x = 0, 0.1, 0.3, 0.5, 0.7, 0.9, 1 were prepared by Pechini and sol-gel methods.

According to the previous work [21], in the Pechini method, the appropriate amounts of $La(NO_3)_3$ (Merck), $Mn(NO_3)_3$ (Merck) and $Ni(NO_3)_2$ (Merck) were dissolved in deionized water (nitrate solution). Then, citric acid (Merck) as a complex agent and ethylene glycol (Merck) were added to the solution one after another with the amount corresponding to the citric acid/total metal ions molar ratio of 2:1 and the ethylene glycol/citric acid mass ratio of 2:3, respectively. To reach higher catalyst activity and higher surface area [21], after that ammonia solution was added dropwise until the pH becomes 1.15 to 1.2. The solution was heated up to 80 ℃ and stirred until the water was evaporated. The formed resin-like precursor was dried at 110 ℃ for 15 h and subsequently calcined in air at 750 ℃ for 4 h.

In the sol-gel method, the nitrate solution was prepared as the same of Pechini method. Citric acid with the molar ratio of 2:1 in respect to the total metal ions was added to the solution. The solution was stirred at 80 $°C$ until the formation of gel-like precursor. The drying and calcination procedure was the same as mentioned above.

2.2 Characterization of catalysts

Fourier-transform infrared spectroscopy (FT-IR) technique was employed to investigate the structure of resin- and gel-like precursors. The dried samples were dissolved in n-hexane and then frozen at -10 $°C$. The obtained crystals were analyzed by FT-IR using Shimadzu 8400s spectrometer. Crystalline structure and lattice parameters were obtained by X-ray diffraction (XRD) analysis using Philips PW-1800 diffractometer. Scanning Electron Microscopy (SEM) was employed to determine the morphologies of the calcined catalysts using a Vega II XMU electron microscope (TESCAN). The specific surface area of the catalysts was determined by the adsorption of nitrogen at -196 ℃ using BELCAT-A apparatus operating in the single-point mode.

2.3. Catalytic activity

The catalytic performance of the prepared catalysts was evaluated in a fixed bed reactor made of stainless-steel tube with an internal diameter of 6 mm. In each run, 200 mg catalyst was charged in the middle of the reactor between two layers of quartz wool and the reactor was placed in a cylindrical furnace. A gas mixture of CH_4/O_2/Ar: 2/10/balanced and CO/O_2/Ar: 2/20/balanced was used as the feed for CH_4 combustion and CO oxidation, respectively. The catalytic measurements were carried out at atmospheric pressure, the temperature range of 200-800 $°C$ and the total gas flow rate of 50 cm^3 (STP)/min.

The feed and product compositions were analyzed by an on-line gas chromatograph (GC) using ThermoFinnigan (KAV00109 series) equipped by thermal conductivity detector (TCD) and 5A 60/80 mesh molecular sieve column.

3. Results and Discussion

3.1. Perovskite stability

The tolerance factor (t) is a criterion factor indicating the preservation and stability of the perovskite structure [26]. t is defined as equation 1.

$$t = \frac{r_A + r_B}{\sqrt{2}(r_B + r_O)} \quad (1)$$

Where r_A, r_B and r_O are the ionic radius of A and B cations and oxygen, respectively. The perovskite structure is stable if $0.8 \leq t \leq 1.0$ [26].

In Figs.1-3, the calculated t factor of the perovskite structure of $LaMn_xNi_{1-x}O_{3\pm\delta}$ is shown. These calculations were performed based on capacities of 2, 3 and 4 for Mn and Ni in the capacities of 2 and 3 for different percentages of substitution.

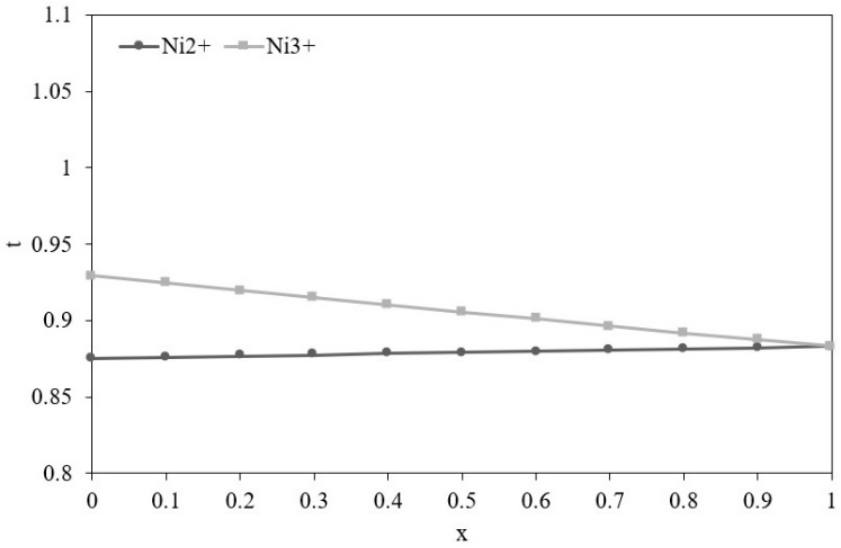

Fig. 1. Tolerance factor for $LaMn_xNi_{1-x}O_{3\pm\delta}$ perovskite with Mn^{2+}, Ni^{+} ions by different capacities.

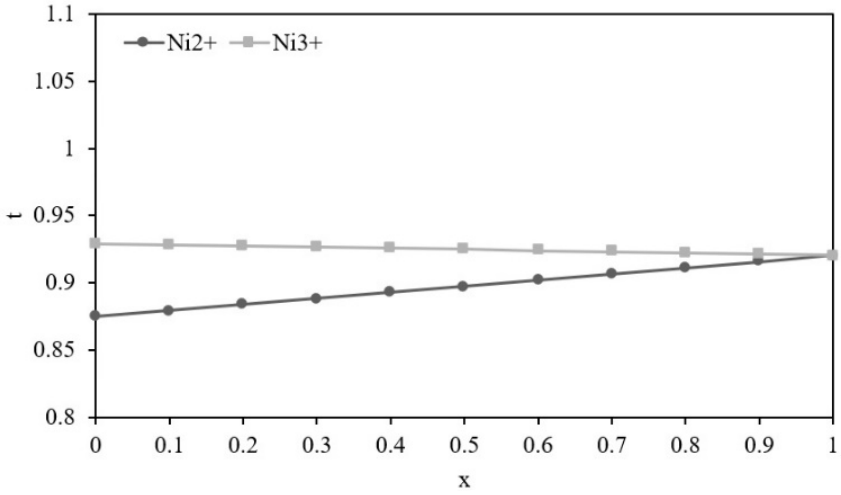

Fig. 2. Tolerance factor for $LaMn_xNi_{1-x}O_{3\pm\delta}$ perovskite with Mn^{3+}, Ni ions by different capacities.

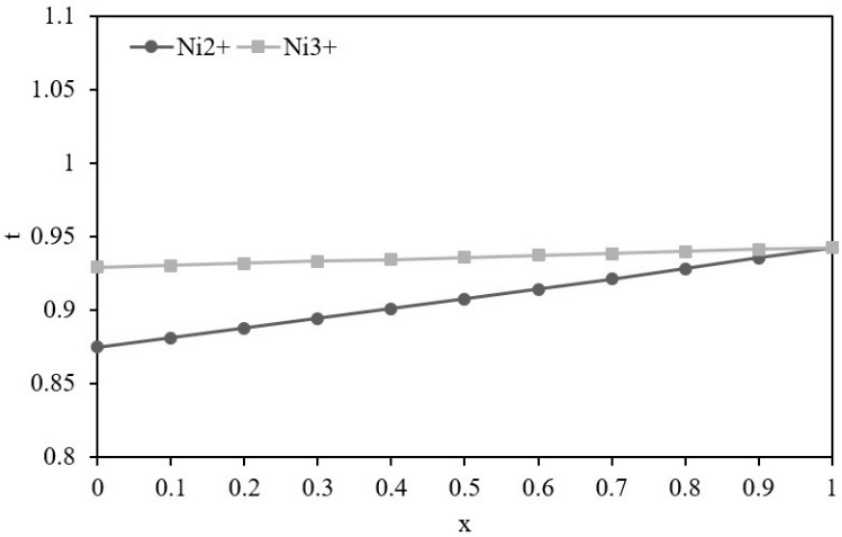

Fig. 3. Tolerance factor for $LaMn_xNi_{1-x}O_{3\pm\delta}$ perovskite with Mn^{4+}, Ni ions by different capacities.

Lanthanum ionic radius of 1.36 Å and load of 3+ are constant in all cases. Considering the stability conditions, perovskite tolerance factors for all nickel and manganese capacities are in the stability limit.

3.2. Characterization of catalysts

FT-IR analysis has been conducted to investigate the bands in the blending and forming gel. The FT-IR of dried gels with different ratios of Mn: Ni prepared by the Pechini method is shown in Fig. 4(a).

A wide band at approximately 3400 cm^{-1} was detected for all Pechini samples and is assigned to hydroxyl groups. The band at 548 cm^{-1} is related to Ni-O bonds in the calcined gel and the formation of nickel oxide. The sharp absorption bands detected at 1190 cm^{-1} and 1730 cm^{-1} are related to monodentate ligands containing a carbonyl group [27]. The band at the range of 860 cm^{-1} indicates the presence of carbonates and nitrates, with some absorption of Ni-O. Therefore, it can be assumed that the CO_3^{2-} derived from the bond of mono-dentate ligands of metal ions with citric acid, exited the gel surface after heating and formed the gaseous compounds. Peaks detected at approximately 1600 cm^{-1} and 1385 cm^{-1} for all samples are attributed to asymmetric and symmetric stretching modes of carbonyl groups, respectively [27, 28]. For the Pechini method, as ethylene glycol is used for polyesterification with citric acid to form a rigid polymer network, a band relating to C-O stretching was detected at approximately 1180 cm^{-1}, confirming the polymerization process [28, 29].

The FT-IR of dried gels with different ratios of Mn: Ni prepared by the sol-gel method is given in Fig. 4(b). A wide band at approximately 3400 cm^{-1} was detected for all samples, and is assigned to hydroxyl groups. The absorption bands detected at 1250 cm^{-1} are related to monodentate ligands containing carbonyl groups. The bands at 604 cm^{-1} also correspond to B-O bond in the octahedral structure of BO_6 in $ABO_{3\pm\delta}$. The band at the range of 844 cm^{-1} indicates the presence of carbonates and some nitrates associated with the absorption of Ni-O. Peaks detected at approximately 1590 cm^{-1} and 1415 cm^{-1} for all samples are attributed to asymmetric and symmetric stretching modes of carbonyl groups, respectively [27, 28]. The FT-IR results thus confirm that the complex formation between citric acid and metallic ions occurred in the sol-gel route and that the polyesterification of ethylene glycol and citric acid and the complexation with metallic ions occurred in the Pechini method. In the sol-gel samples, the bands near 844 cm^{-1}, 1415 cm^{-1} and 1590 cm^{-1} are related to carbonate, nitrate carbonyl groups which are moved from 860 cm^{-1} to 844 cm^{-1}, 1385 cm^{-1} to 1415 cm^{-1} and 1600 cm^{-1} to 1590 cm^{-1}.

As mentioned above, the perovskite structure is crystal in the same base by two diamond-faces. Thus, perovskite structures are assumed as a cubic lattice in many reviews. Peak locations of $LaMn_xNi_{1-x}O_{3\pm\delta}$ samples remained perfect by the introduction of Ni^{3+}, implying the completion of crystallization. Meanwhile, the maximum peak of XRD patterns of the doping sample is weakened and broader, indicating that $LaMn_xNi_{1-x}O_{3\pm\delta}$ is a single phase with more rhombohedral distorted perovskite structures than undoped samples of $LaMnO_3$.

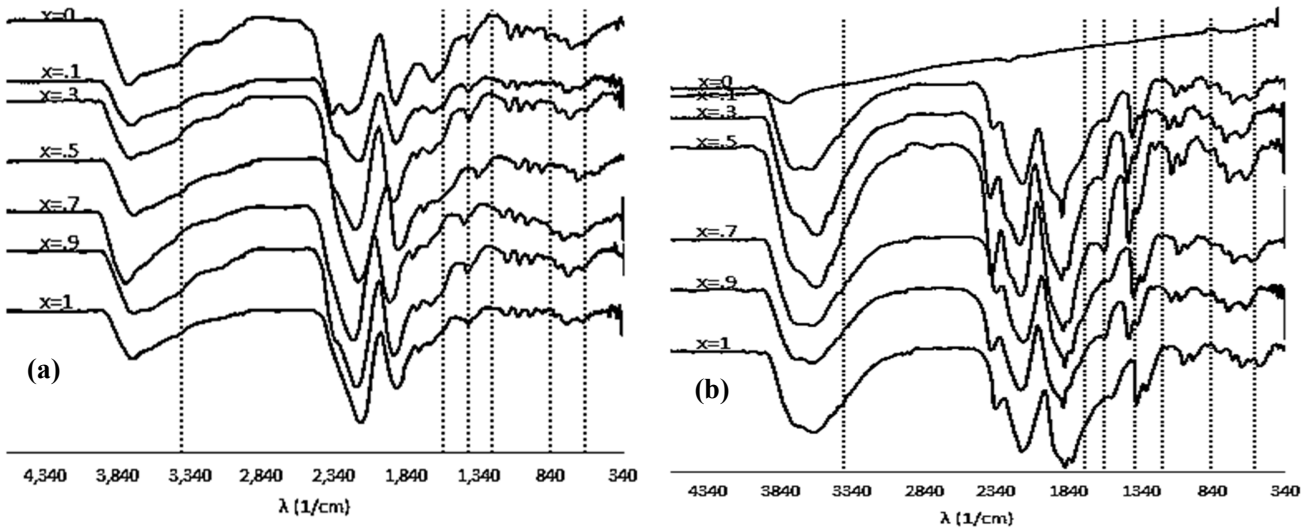

Fig. 4. FT-IR spectra and bands of the gel of $LaMn_xNi_{1-x}O_{3\pm\delta}$ dried at 110 ℃, prepared by the Pechini method (a) and the sol-gel method (b).

The XRD patterns of the prepared catalysts are shown in Fig. 5. It can be seen that for all $LaMn_xNi_{1-x}O_{3\pm\delta}$ compositions, well crystallized perovskite was obtained by both two methods. For Pechini samples, especially in more substitutions of nickel, additional peaks were found at 26.2° and 28.6° which represent the formation of La_2O_3 and Mn_6O_{12}. It suggests that the addition of Ni^{3+} induced the loss of A-site cation and produced a cation vacancy. In fewer substitutions of nickel, the perovskite phase is well identified.

As indicated in Fig. 5(b), there is no peak of secondary phases or starting agents in most sol-gel samples, showing that all transition metals are completely dissolved in the perovskite structure. As already observed, the perovskite phase is the main phase in all samples.

The XRD results indicate that the Pechini leads to richer and stronger perovskite phases and the calcined product has a high degree of crystallization (Table 1).

According to previous studies, Cr, Fe or Mn-containing perovskites exhibit an orthorhombic structure, whereas Co and Ni-containing perovskites display a rhombohedra structure [30]. Consequently, as seen in the XRD patterns, the maximum XRD peak of samples which replace nickel becomes weaker and wider, indicating that $LaMnO_{3\pm\delta}$ has an orthorhombic structure, while the samples with higher replacements of nickel gradually deform from an orthorhombic to a rhombohedra structure in comparison to the $LaMnO_{3\pm\delta}$ sample.

An enlargement of the area in the XRD spectrum for 2θ of between 32° and 34°, where the sharpest peak appeared, shows some shifts (Fig. 6).

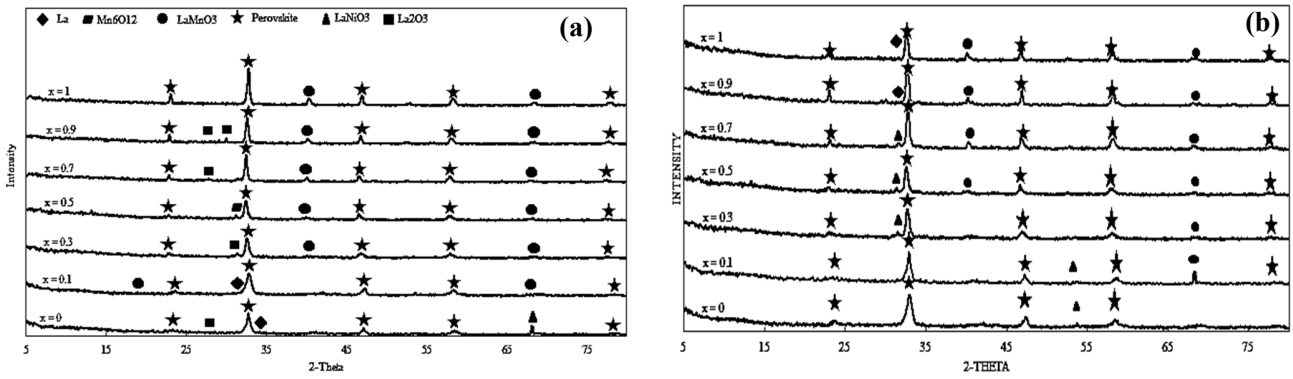

Fig. 5. XRD patterns of $LaMn_xNi_{1-x}O_{3\pm\delta}$ prepared by the Pechini method (a) and the sol-gel method (b).

Table 1. Crystallite sizes of the prepared perovskites.

Preparation method	Perovskite structure	Crystal size (nm)
Pechini	$LaNiO_{3\pm\delta}$	19.52
	$LaMn_{0.1}Ni_{0.9}O_{3\pm\delta}$	23.98
	$LaMn_{0.3}Ni_{0.7}O_{3\pm\delta}$	21.14
	$LaMn_{0.5}Ni_{0.5}O_{3\pm\delta}$	22.64
	$LaMn_{0.7}Ni_{0.3}O_{3\pm\delta}$	23.5
	$LaMn_{0.9}Ni_{0.1}O_{3\pm\delta}$	22.94
	$LaMnO_{3\pm\delta}$	25.02
Sol-gel	$LaNiO_{3\pm\delta}$	16.32
	$LaMn_{0.1}Ni_{0.9}O_{3\pm\delta}$	23.64
	$LaMn_{0.3}Ni_{0.7}O_{3\pm\delta}$	22.42
	$LaMn_{0.5}Ni_{0.5}O_{3\pm\delta}$	22.4
	$LaMn_{0.7}Ni_{0.3}O_{3\pm\delta}$	22.88
	$LaMn_{0.9}Ni_{0.1}O_{3\pm\delta}$	30.56
	$LaMnO_{3\pm\delta}$	28.78

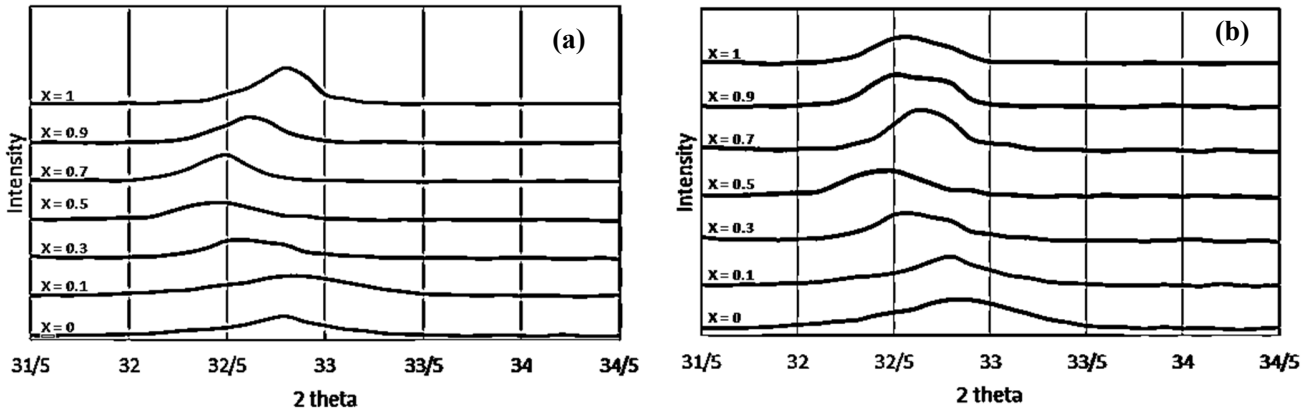

Fig. 6. Evolution of the position of the XRD highest peak for $LaMn_xNi_{1-x}O_{3\pm\delta}$ samples prepared by the Pechini method (a) and the sol-gel method (b).

Although different peaks were expected when adding Mn to the $LaNiO_3$ structure, the regular decrease in the main peak shows that this element entered the perovskite structure during calcination at 750 °C and 4 h. Since the ionic radius of Mn^{3+} is larger than that of Ni^{3+}, lattice parameters are increased by Mn addition. In addition, it can be seen from Fig. 6 that XRD diffraction peak shifted toward the upper 2θ by Mn addition. It indicates that the reduction of Mn^{4+} to Mn^{3+} causes a decrease in the unit cell volume due to the differences between the ionic radius of Mn^{4+} and Mn^{3+}. The obtained results revealed that the last two peaks are corresponding to the reduction of non-stoichiometric excess oxygen and Mn^{4+}.

The lattice parameter (A) was calculated from the five most intense diffraction lines. The results are shown in Fig. 7. The structure was assumed to be a pseudo-cubic. According to results shown in Fig. 7, the lattice parameter for the sample of interest, especially to x=0.5, changes linearly. For Pechini samples, the lattice parameter decreased with increasing Mn, especially by the substitution of $0\leq x\leq 0.5$, but no correlation was observed for sol-gel samples. Because the sol-gel method yields a greater separation of Mn from the perovskite structure. Lower Mn segregation in Pechini samples is due to the usage of ethylene glycol which leads to the formation of a rigid polymer network that suppresses the mobility of metal–citric acid complexes, minimizing the segregation of metal particles during calcination. The obtained curve can be used as a calibration in order to evaluate the Mn content and/or migration of Ni out of the structure during the reaction.

To estimate the homogeneity of the obtained solid solution, $LaMn_xNi_{1-x}O_{3\pm\delta}$ perovskites were examined by SEM, as shown in Fig. 8. According to Fig. 8, Pechini samples have more porous structures than sol-gel samples, while samples with almost straight faces were observed in the sol-gel samples. As the degree of substitution increases in $LaMn_xNi_{1-x}O_{3\pm\delta}$, the macro porosity also increases. The morphology changes due to the formation of solids with more stoichiometric defects, as observed by XRD (Fig. 5).

The contained particles have a distribution of small particles (~70-120 nm) in Pechini samples due to their porosity, while the sol-gel contained particles have a distribution of larger particles (~150-200 nm). In addition, a more uniform particle size distribution is seen in Pechini samples. The smaller particle size in Pechini samples can result in a larger surface area than the sol-gel samples. Thus, Pechini samples can have higher catalytic activity compared to sol-gel samples.

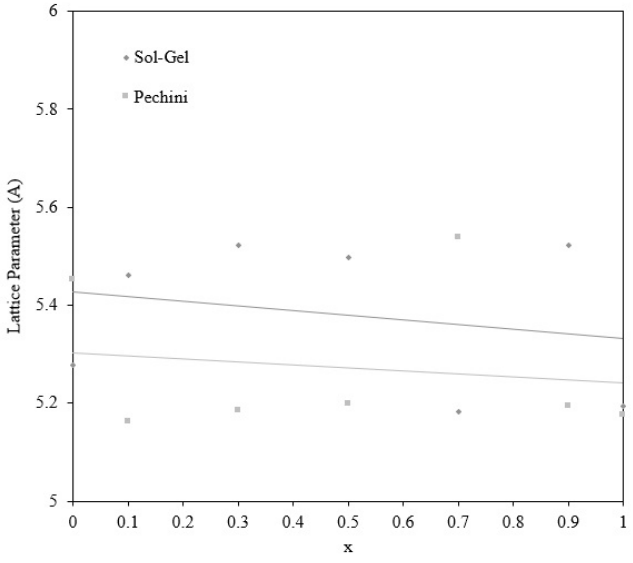

Fig. 7. Lattice parameters of the pseudo-cubic structure of $LaMn_xNi_{1-x}O_{3\pm\delta}$ samples.

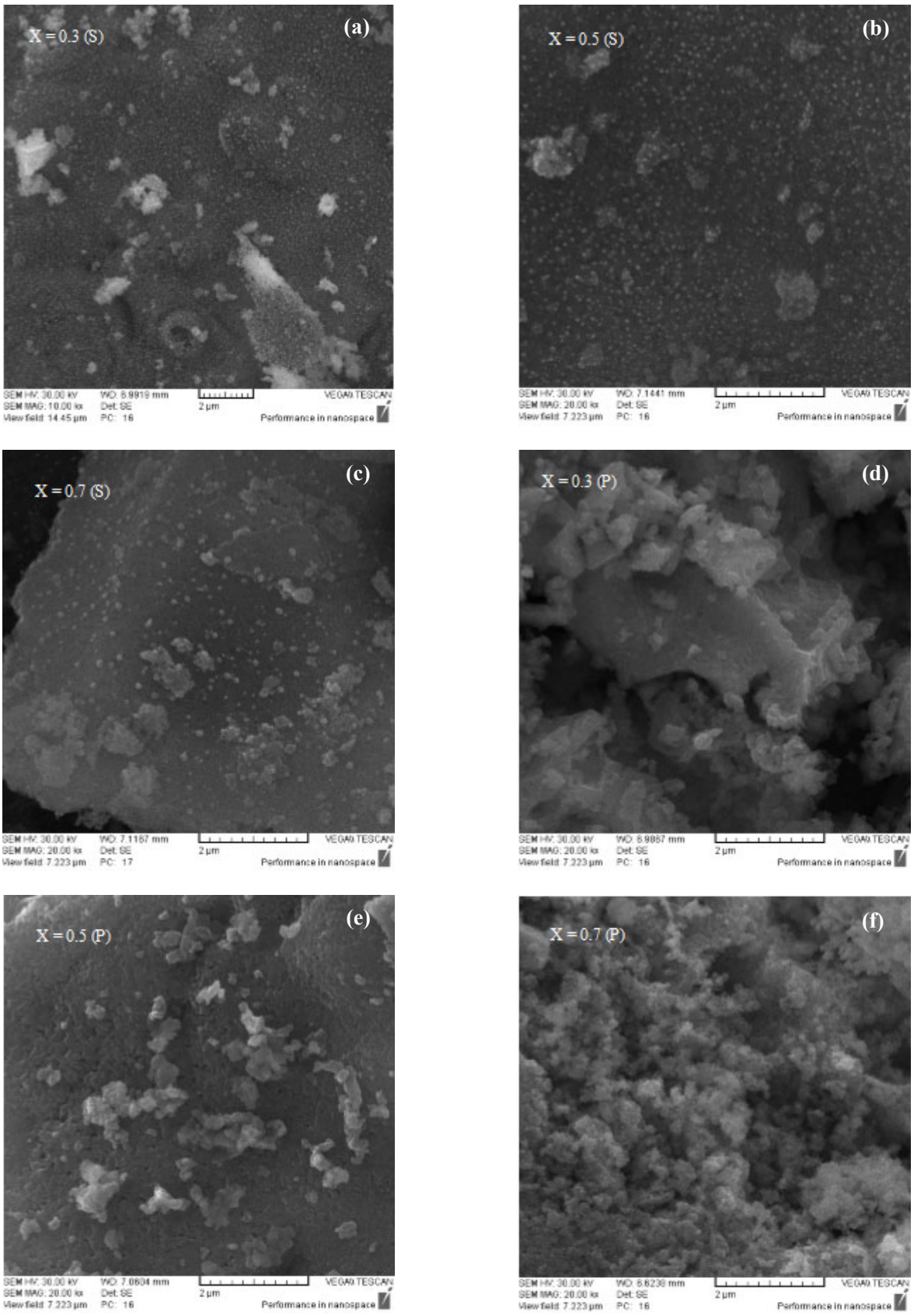

Fig. 8. SEM micrographs of $LaMn_xNi_{1-x}O_{3\pm\delta}$ prepared by the Pechini (P) and sol-gel (S) methods at three different values of x.

In Pechini samples, especially by fewer replacements of Ni (samples x=0.1 to x=0.3), foamy agglomerated grains are exhibited with a wide distribution and presence of voids in their structure due to large escaped gas evolution.

Based on the literature [3, 7, 8], it can be explained that the presence of organic molecules plays two critical roles in the perovskite structure. The organic molecules produce complexes with metal nitrates and provide homogeneity of the sol-gel via avoiding the precipitation of ionic species. In addition, the porous and lamellar-structured samples is formed due to the combustion of the resulting gel during the calcination at high temperatures. The Pechini method allows for easy control over the final stoichiometry and low processing temperatures, without intermediate grindings.

The surface area of the catalyst is an important factor in catalytic properties. For instance, the higher catalytic activity of the catalysts can result from their higher surface area. The BET surface areas of the samples are summarized in Table 2. All perovskite samples prepared by the Pechini method had greater surface areas than samples prepared by the sol-gel method. All substitutions from x=0.3 decreased the surface area of $LaMnO_3$ in Pechini and sol-gel samples. The $LaMn_{0.3}Ni_{0.7}O_3$ sample prepared by the Pechini method has the largest surface area (10 m^2/g) due to its lower particle size and a more porous structure. Its particle size is larger than the crystal domain size calculated from XRD data, presumably due to agglomeration. The agglomeration extent becomes more pronounced with increasing the calcination temperature. The XRD and BET results show that the samples prepared form a series of crystalline $LaMn_xNi_{1-x}O_{3\pm\delta}$ phases that have similar structures but surface areas that vary over a wide range.

3.3. CH_4 combustion and CO oxidation

The activity of the catalysts in CH_4 combustion and CO oxidation was investigated in the temperature range of 400-750 ℃ and 50-350 ℃, respectively. The results are shown in Fig. 9. It can be seen that CH_4 and CO conversion increased with the introduction of Ni in the perovskite structure. It reached a maximum point then further increase in Ni content reduced the catalytic activity. The maximum CH_4 conversion was at x = 0.3 for samples prepared by the Pechini method, and at x = 0.7 for samples prepared by the sol-gel method. $LaMn_{0.3}Ni_{0.7}O_3$ exhibited the highest activity for CO oxidation and only CO_2 was detected in the products.

The activity of the samples has been influenced by both structural deficiency and the number of active sites. By substituting nickel in the structure, a structure defect has been made in the perovskite network because of the ionic charge difference on B site elements. On the other hand, the number of Mn sites which is more active than Ni, decreases. Therefore, to achieve the maximum activity, an optimum Ni content should be used.

Table 2. BET surface areas of $LaMn_xMi_{1-x}O_{3\pm\delta}$ samples.

Preparation method	Perovskite structure	Surface area (m^2/g)
Pechini	$LaNiO_{3\pm\delta}$	5
	$LaMn_{0.1}Ni_{0.9}O_{3\pm\delta}$	6.5
	$LaMn_{0.3}Ni_{0.7}O_{3\pm\delta}$	10
	$LaMn_{0.5}Ni_{0.5}O_{3\pm\delta}$	8.9
	$LaMn_{0.7}Ni_{0.3}O_{3\pm\delta}$	8.8
	$LaMn_{0.9}Ni_{0.1}O_{3\pm\delta}$	8.3
	$LaMnO_{3\pm\delta}$	8.5
Sol-gel	$LaNiO_{3\pm\delta}$	3
	$LaMn_{0.1}Ni_{0.9}O_{3\pm\delta}$	4.2
	$LaMn_{0.3}Ni_{0.7}O_{3\pm\delta}$	6.4
	$LaMn_{0.5}Ni_{0.5}O_{3\pm\delta}$	6.3
	$LaMn_{0.7}Ni_{0.3}O_{3\pm\delta}$	6.2
	$LaMn_{0.9}Ni_{0.1}O_{3\pm\delta}$	6
	$LaMnO_{3\pm\delta}$	5.8

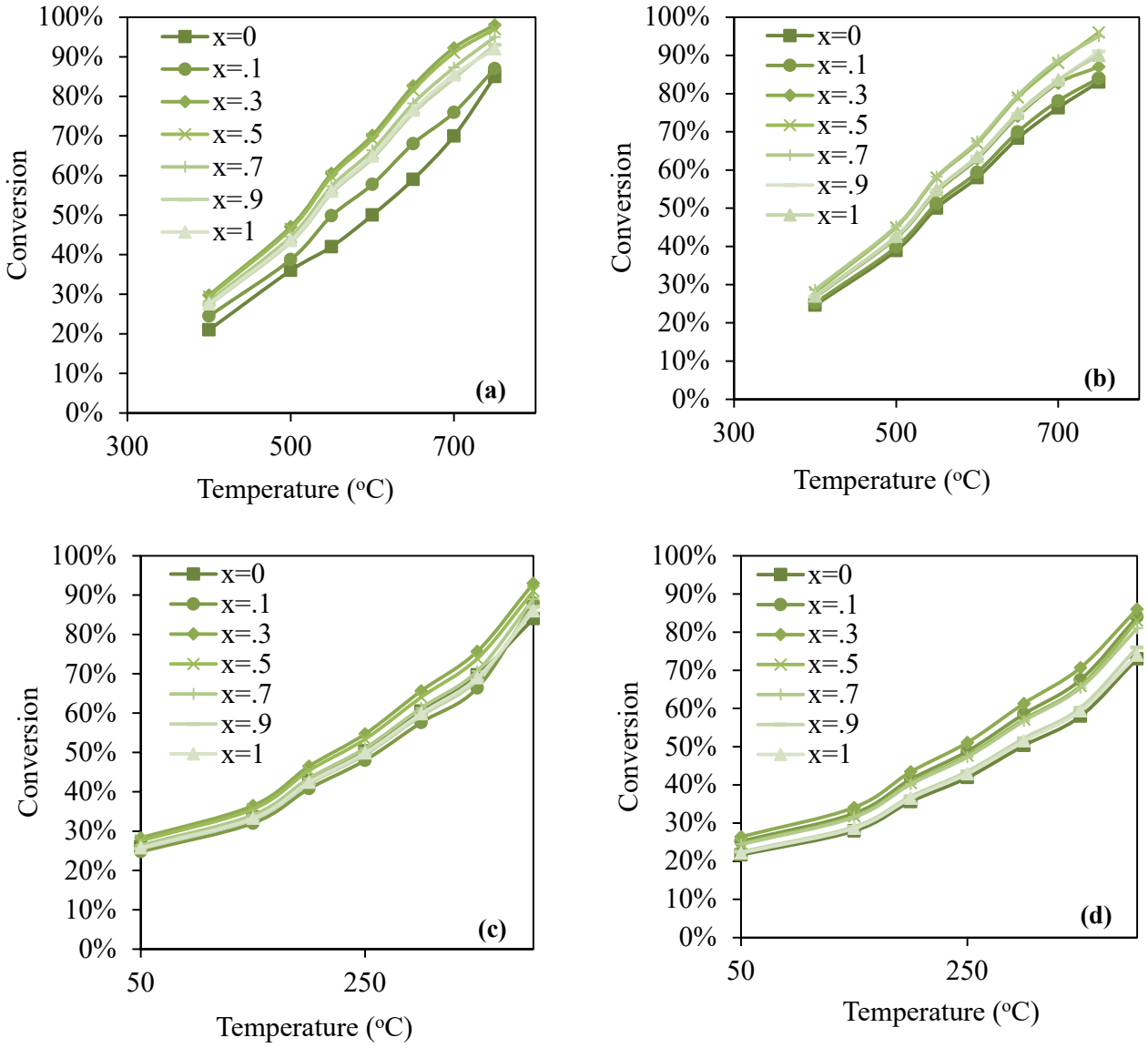

Fig. 9. Catalytic activity of $LaMn_xMi_{1-x}O_{3\pm\delta}$ prepared by the Pechini method (a,c) and sol-gel method (b,d) for CH_4 combustion (a,b) and CO oxidation (c,d) (atmospheric pressure, F= 50 mL/min, 200 mg catalyst).

The obtained $T_{60\%}$ for all samples are shown in Table 3. It can be concluded that the Pechini samples showed higher catalytic activity as compared to the sol-gel method. Both the CH_4 conversion and CO oxidation occurred at lower temperatures for the samples prepared by the Pechini method. It can be due to the smaller particle size and higher surface area of the Pechini samples.

3.4. Stability test

The stability of $LaMn_{0.3}Ni_{0.7}O_3$ catalyst prepared by Pechni method was investigated at both CH_4 combustion and CO oxidation. The experiments were performed at the temperature of 750 °C for 100 h.

The CH_4 and CO conversion as a function of reaction time is shown in Fig. 10.

The catalyst exhibited almost stable performance and the decrease in the CH_4 and CO conversion were negligible during 100 h time on stream. However, successive increases and decreases in catalyst activity have been recorded. The reduction in the activity may be attributed to the increase in the average oxidation state. The increase in the catalytic activity may be due to the oxidation of metallic Ni to Ni^{2+} and its penetrating to the perovskite structure. In CH_4 combustion, the CH_4 conversion decreased from 98 to 93%. In CO oxidation, the CO conversion decreased from 93 to 87%.

Table 3. $T_{60\%}$ of $LaMn_xMi_{1-x}O_{3\pm\delta}$ in CH_4 combustion and CO oxidation.

Preparation method	x	$T_{60\%}$ (°C)	
		CH_4	CO
Pechini	0	655.3	299.9
	0.1	611.5	316.8
	0.3	547.7	274.6
	0.5	550.7	281.9
	0.7	564.0	294.4
	0.9	574.4	304.3
	1	571.5	300.5
Sol-gel	0	610.3	358.6
	0.1	604.1	308.9
	0.3	583.7	293.9
	0.5	561.2	318.3
	0.7	559.5	320.2
	0.9	579.4	349.4
	1	581.2	352.9

As shown in Tables 4 and 5, it is observed that the $LaMn_xNi_{1-x}O_{3\pm\delta}$ perovskite catalyst prepared in this work showed a higher activity, especially in CO oxidation, in comparison with previous studies on the combustion of CH_4 and CO oxidation. A higher activity was observed in $LaMnO_3$ and $LaNiO_3$ perovskites in CO oxidation reactions as compared with other perovskites. Moreover, with the substitution of nickel in lanthanum manganite to x = 0.7, it can be claimed that it had one of the highest activities. But comparing different results is difficult. Because selected experimental conditions are different. The method of preparation, the element of A and B in the structure of LaABO perovskite, GHSV and composition of feed are important parameters to compare the activity and $T_{60\%}$ of perovskite catalyst with each other. So, an attempt was made to select previous works that have similar conditions of reaction (GHSV and Feed composition) with this work.

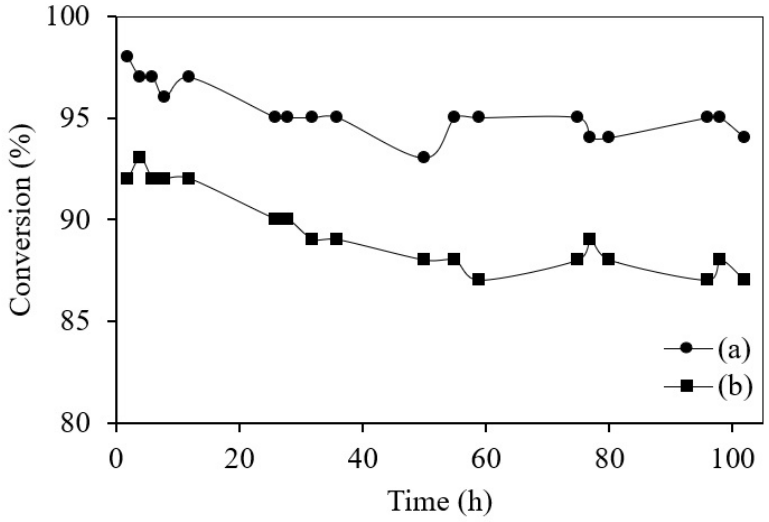

Fig. 10. Stability of $LaMn_{0.3}Ni_{0.7}O_{3\pm\delta}$ prepared by the Pechini method for CH_4 combustion (a) and CO oxidation (b) (T= 750 ℃, atmospheric pressure, F= 50 mL/min, 200 mg catalyst).

Table 4. Comparison of $T_{60\%}$ in CH_4 combustion reaction of $LaMn_{.3}Ni_{.7}O_3$ by other research catalysts.

Catalyst	Feed Composition	GHSV ($Ncm^3/(g.h)$)	$T_{60\%}$ (°C)	Ref.
$LaMn_{0.3}Ni_{0.7}O_3$, Pechini Method	2 % CH_4, 10 % O_2, N_2 Balance	15000	548.5	This work
$LaMn_{0.3}Ni_{0.7}O_3$, Sol-gel Method	2 % CH_4, 10 % O_2, N_2 Balance	15000	572	This work
$LaMnO_3$	2 % CH_4, in the air	45000	601	[13]
$LaMn_{0.8}Cu_{0.2}O_3$	2 % CH_4, 10 % O_2, N_2 Balance	15000	593	[31]
La_2CuNiO_6	2 % CH_4, 18 % O_2, N_2 Balance	24000	581.25	[34]
$LaMn_{0.8}Al_{0.2}O_3$	0.4 % CH_4, 10 % O_2, N_2 Balance	40000	776	[37]
$LaAlO_3$	0.4 % CH_4, 10 % O_2, N_2 Balance	40000	943.5	[37]

According to the literature [31-38], The reason of thehigh activities of $LaMn_xNi_{1-x}O_{3\pm\delta}$ perovskite oxide can be attributed to the high density of lanthanum nickel**.** In addition, the inherent tendency of Mn^{3+} to oxidize to Mn^{4+} during heating in air resulted in cation vacancies and the presence of δ excess oxygen compared to the stoichiometric. Also, the electrical conductivity of nickel can be a very important feature of perovskites as a prerequisite for high activity.

4. Conclusions

The $LaMn_xNi_{1-x}O_{3\pm\delta}$ (x = 0, 0.1, 0.3, 0.5, 0.7, 0.9, 1) perovskite catalysts were prepared by the sol-gel and the Pechini methods, characterized and tested in the CH_4 and CO oxidation. The Ni content and also the preparation method was proved to be important parameters affecting the catalyst structure and performance. The Pechini samples are more active than the sol-gel samples due to the higher surface area, smaller particle size and more homogeneity obtained by the Pechini method.

Ni content influences the catalytic performance through 1. structural defect, 2. reducing the number of active sites. Structural defect can form oxygen vacancies or change oxidation state of B cation; this leads to the influencing on oxygen mobility, and therefore, increasing the catalytic performance. On the other hand, Mn is more active than Ni. Hence partially substituted Ni in the perovskite structure can reduce the activity.

The $LaMn_{0.3}Ni_{0.7}O_{3\pm\delta}$ perovskite exhibits the highest CH_4 and CO conversions than other samples. The comparison of $LaMn_xNi_{1-x}O_{3\pm\delta}$ with previous studies shows higher activity and stability.

References

[1] Z. Li, G.B. Hoflund, J. Nat. Gas Chem. 12 (2003) 153-160.
[2] H. He, M. Liu, H. Dai, W. Qiu, X. Zi, Catal. Today 126 (2007) 290-295.
[3] S. Ordóñez, J.R. Paredes, F.V. Díez, Appl. Catal. A 341 (2008) 174-180.
[4] J.H.G. Rangel, P.R.G. Gonçalves Jr, M.M. Oliveira, M.I.B. Bernardi, Elson Longo, L.E.B. Soledade, I.M.G. Santos, A.G. Souza, Mater. Res. Bull. 43 (2008) 825-835.
[5] S. Cimino, A. Di Benedetto, R. Pirone, G. Russo, Catal. Today 83 (2003) 33-43.
[6] R. Spinicci, A. Delmastro, S. Ronchetti, A. Tofanari, Mater. Chem. Phys. 78 (2003) 393-399.
[7] S. Cimino, S. Colonna, S. De Rossi, M. Faticanti, L. Lisi, I. Pettiti, P. Porta, J. Catal. 205 (2002) 309-317.
[8] C. Gong, F. Guoliang, H. Yanfeng, S. Chonglin, H. Qifei, Z. Zhongrong, Front. Chem. Sci. Eng. 1 (2007) 6-10.
[9] G. Xu, H. Bai, X. Huang, W. He, L. Li, G. Shen, G. Han, J. Mater. Chem. A 3 (2015) 547-554.
[10] E. Campagnoli, A. Tavares, L. Fabbrini, I. Rossetti, Y.A. Dubitsky, A. Zaopo, L. Forni, Appl. Catal. B 55 (2005) 133-139.
[11] X. Yan, Q. Huang, B. Li, X. Xu, Y. Chen, S. Zhu, S. Shen, J. Ind. Eng. Chem. 19 (2013) 561-565.

Table 5. Comparison of $T_{60\%}$ in CO oxidation reaction of $LaMn_{.3}Ni_{.7}O_3$ by other research catalysts.

Catalyst	Feed Composition	GHSV ($Ncm^3/(g.h)$)	$T_{60\%}$(°C)	Ref.
$LaMn_{0.3}Ni_{0.7}O_3$, Pechini method	2 % CO, 20 % O_2, N_2 Balance	15000	276	This work
$LaMn_{0.3}Ni_{0.7}O_3$, sol-gel method	2 % CO, 20 % O_2, N_2 Balance	15000	295	This work
$LaMn_{0.8}Al_{0.2}O_3$	1 % CO, 20 % O_2, N_2 Balance	12000	408.25	[37]
$LaAlO_3$	1 % CO, 20 % O_2, N_2 Balance	12000	758.5	[37]

[12] H. Ziaei-Azad, A. Khodadadi, P. Esmaeilnejad-Ahranjani, Y. Mortazavi, Appl. Catal. B 102 (2011) 62-70.
[13] Y. Ding, S. Wang, L. Zhang, Z. Chen, M. Wang, S. Wang, Catal. Commun. 97 (2017) 88-92.
[14] Z. Zhang, Z. Kong, H. Liu, Y. Chen, Front. Chem. Sci. Eng. 8 (2014) 87-94.
[15] J. Yang, Y. Guo, Chinese Chem. Lett. 29 (2018) 252-260.
[16] K.S. Song, H.X. Cui, S.D. Kim, S.K. Kang, Catal. Today 47 (1999) 155-160.
[17] C. Shi, H. Chang, C. Wang, T. Zhang, Y. Peng, M. Li, Y. Wang, J. Li, Ind. Eng. Chem. Res. 57 (2018) 920-926.
[18] Y. Shao, X.F. Wang, M. Ao, C.R. Gong, G.L. Fan, H.F. Chen, Front. Mater. Sci. 6 (2012) 304-310.
[19] W. Yue-Hui, L. Lai-Tao, L. Wei, Russ. J. Phys. Chem. A 84 (2010) 405-408.
[20] R.J.H. Voorhoeve, D.W. Johnson, J.P. Remeika, P.K. Gallagher, Science 195 (1977) 827-833.
[21] R. Ran, X. Wu, D Weng, J. Alloys Comp. 414 (2006) 169-174.
[22] H. Falcón, J.A. Barbero, J.A. Alonso, M.J. Martínez-Lope, J.L.G. Fierro, Chem. Mater. 14 (2002) 2325-2333.
[23] L.G. Tejuca, J.L.G. Fierro, J.M. Tascón, Adv. Catal. 36 (1989) 237-328.
[24] S. Royer, D. Duprez, ChemCatChem 3 (2011) 24-65.
[25] T. Seiyama, Catal. Rev. 34 (1992) 281-300.
[26] M. Parvary, S.H. Jazayeri, A. Taeb, C. Petit, A. Kiennemann, Catal. Commun. 2 (2001) 357-362.
[27] H. Arai, T. Yamada, K. Eguchi, T. Seiyama, Appl. Catal. 26 (1986) 265-276.
[28] A.C. Terracciano, S.T. De Oliveira, S.S. Vasu, N. Orlovskaya, Exp. Therm. Fluid Sci. 90 (2018) 330-335.
[29] D.A. Hassan, J. Xu, Y. Chen, L. Li, R. Zeng, Mater. Res. Bull. 79 (2016) 69-72.
[30] H. Wang, X. Dong, T. Zhao, H. Yu, M. Li, Appl. Catal. B 245 (2019) 302-313.
[31] R. Benakcha, M. Omari, Inorg. Nano-Met. Chem. 47 (2017) 1103-1109.
[32] G. Saracco, G. Scibilia, A. Iannibello, G. Baldi, Appl. Catal. B 8 (1996) 229-244.
[33] M. Haruta, H. Sano, Int. J. Hydrogen Energ. 7 (1982) 737-740.
[34] R. Hu, R. Ding, J. Chen, J. Hu, Y. Zhang, Catal. Commun. 21 (2012) 38-41.
[35] G. Saracco, F. Geobaldo, G. Baldi, Appl. Catal. B 20 (1999) 277-288.
[36] Z. Zhong, K. Chen, Y. Ji, Q. Yan, Appl. Catal. A 156 (1997) 29-41.
[37] C.A. da Silva, P.E.V. de Miranda, Int. J. Hydrogen Energy 40 (2015) 10002-10015.
[38] A.C. Terracciano, S.T. De Oliveira, S.S. Vasu, N. Orlovskaya, Exp. Therm. Fluid Sci. 90 (2018) 330-335.